

Sb₂S₃-Sensitized Photoelectrochemical Cells: Open Circuit Voltage Enhancement through the Introduction of Poly-3-hexylthiophene Interlayer

Jin Hyuck Heo,^{†,‡,§} Sang Hyuk Im,^{†,§} Hi-jung Kim,[†] Pablo P. Boix,[§] Suk Joong Lee,[‡] Sang Il Seok,^{*,†} Iván Mora-Seró,^{*,§} and Juan Bisquert^{*,§}

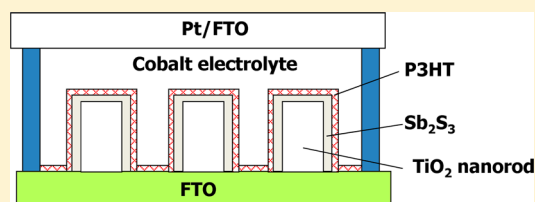
[†]Solar Energy Materials Research group, Advanced Materials Division, Korea Research Institute of Chemical Technology, 141 Gajeong-ro, Yuseong-gu, Daejeon 305-600, Korea

[‡]Department of Chemistry, Korea University, Seoul, 136-701 Republic of Korea

[§]Photovoltaic and Optoelectronic Devices Group, Departament de Física, Universitat Jaume I, 12071 Castelló, Spain

Supporting Information

ABSTRACT: The Sb₂S₃-sensitized photoelectrochemical cells (Sb₂S₃-SPECs) in cobalt electrolyte were fabricated by depositing Sb₂S₃ on the macroporous TiO₂ nanorods electrodes and consecutively spin-coating P3HT (Poly-3-hexylthiophene) interlayer to relieve the mass transport problem at vicinity of Sb₂S₃ and cobalt redox couples and reduce the backward recombination. Through the introduction of P3HT interlayer, we could greatly enhance the power conversion efficiency of Sb₂S₃-SPEC to 4.2% at 1 sun illumination, whereas the Sb₂S₃-SPEC without P3HT interlayer exhibits 3.2% of device efficiency. The electrochemical impedance analysis let us know that the improved device performance was mainly attributed to the reduced backward recombination building up the higher open circuit voltage.



1. INTRODUCTION

Dye-sensitized photoelectrochemical cells (D-SPECs) have been considered to be a cost-effective alternative to conventional semiconductor-based solar cells because Grätzel et al. developed highly efficient PECs with ~11% of power conversion efficiency at 1 sun illumination.^{1–3} Therefore, very intensive studies have been done to attain more than 11% of power conversion efficiency in D-SPECs using iodide redox electrolyte for two decades, but further improvement of device performance was very difficult with this redox couple. It is certain that iodide redox couple is an excellent electrolyte from the point of view of recombination, but its energy position limits the open circuit potential of D-SPECs.⁴

Because Feldt et al.⁵ reported highly efficient D-SPECs using cobalt redox electrolyte, new light has begun to be shed on the cobalt redox couples. Very recently Yella et al.⁶ succeeded to fabricate ~12% of zinc porphyrin complex D-SPECs using cobalt redox electrolyte under 1 sun illumination, and Yum et al.⁷ reported that the cobalt redox shuttles could build up the open circuit voltage up to >1000 mV.

In parallel, inorganic semiconductors or quantum dots (QDs) have also received great attention as a promising candidate for replacing conventional Ru/organic dyes in D-SPECs due to their prominent properties such as a high absorption coefficient, large intrinsic dipole moment, convenient bandgap tunability, multiple exciton generation, and good stability.⁸ Among metal chalcogenide semiconductors such as CdS(e),^{9–14} PbS(e),^{15–17} and Sb₂S₃,^{18–25} the Sb₂S₃ seems to be a very promising choice to attain high device performance

because it has strong extinction coefficient at the visible region and suitable energy bandgap.^{26–28} The efficient all solid-state Sb₂S₃-sensitized¹⁹ or extreme thin absorber (ETA)¹⁸ solar cells have been successfully demonstrated, and recently we reported on the solid-state Sb₂S₃-sensitized heterojunction solar cells of over 6% of power conversion efficiency at 1 sun illumination.^{22–24} However, the efficient Sb₂S₃-SPECs have rarely been reported until now except our previous reports^{29,30} due to the quick corrosion reactions of Sb₂S₃ with conventional iodide or polysulfide electrolyte.²⁹

Owing to the stronger absorption and bulkier dimension of Sb₂S₃ than Ru dyes attached on the TiO₂ surface, we have found that the cobalt redox shuttles undergo mass transport problem at the vicinity of Sb₂S₃/electrolyte interface in pore space within mesoscopic TiO₂ electrode. The poly-3-hexylthiophene (P3HT) hole buffer interlayer between TiO₂/Sb₂S₃ and cobalt electrolyte accelerates hole extraction from Sb₂S₃ to P3HT having extended effective interface area²⁹ and can relieve the mass transport limitation of cobalt redox shuttles. Although the cobalt redox shuttles can hold high open circuit voltage, the mesoscopic Sb₂S₃-SPECs (having P3HT hole buffer interlayer) have exhibited only ~500 mV of open circuit voltage owing to sluggish transport of cobalt redox shuttles in the random nanoparticulate TiO₂ network producing increased recombination. To relieve the mass transport problem at

Received: May 27, 2012

Revised: August 25, 2012

Published: August 30, 2012

vicinity of Sb_2S_3 and cobalt redox couples and reduce the backward recombination in Sb_2S_3 -SPECs, we used TiO_2 NRs photoelectrode as a macroporous model electrode instead of conventional mesoporous TiO_2 and introduced P3HT interlayer in between Sb_2S_3 -sensitizer and cobalt electrolyte. This architecture aims to speed up both hole extraction from the absorber and its transport via uninterrupted pathway of the redox species to the counterelectrode avoiding recombination losses. Here we could significantly improve the performance of Sb_2S_3 -SPEC by the combination of macroporous TiO_2 NRs electron conductor and P3HT interlayer.

2. EXPERIMENTAL SECTION

Preparation of TiO_2 NRs Electron Conductor. We prepared the TiO_2 NRs as described in the literature.³¹ Typically, we first deposited a 50 nm thick TiO_2 blocking layer (bl- TiO_2) on F-doped SnO_2 (FTO, Pilkington, TEC8) glass plates by spraying 20 mM of titanium diisopropoxide bis(acetylacetonate) (Aldrich) solution at 450 °C to prevent direct contact of the FTO electrode from cobalt electrolyte. We then deposited a ZnO seed layer on bl- TiO_2 /FTO substrate by dip-coating in 0.1 M zinc acetate dihydrate (ACS reagent, $\geq 98\%$)/ethanol solution placed on hot plate set to 90 °C and subsequent heat treatment at 450 °C for 30 min. The sacrificial ZnO NRs were then grown by immersing the ZnO seeds/bl- TiO_2 /FTO substrate in 0.015 M zinc nitrate hexahydrate (ACS reagent, 98%) and 0.015 M hexaethylenetetramine (ACS reagent, 99+%) aqueous solution at 95 °C for 12 h. To convert the ZnO NRs into TiO_2 NRs, we immersed the ZnO NR films in 0.075 M ammonium hexafluorotitanate (Aldrich) and 0.2 M boric acid (Yakuri Pure Chemicals) aqueous solution at 30 °C for 1.5 h. We soaked the TiO_2 NRs film in 40 mM TiCl_4 aqueous solution at 60 °C for 1 h to remove completely the residual ZnO and improve the interfacial contact between TiO_2 NRs and the bl- TiO_2 film. Finally, we heat-treated it at 450 °C for 30 min to make crystalline TiO_2 NRs.

Deposition of Sb_2S_3 -Sensitizer. To form the Sb_2S_3 -sensitizer on the TiO_2 NRs film (diameter = ~ 70 nm, length = ~ 1 μm , crystalline phase = anatase), we conducted chemical bath deposition (CBD)^{27–29} for 2.5 h using a solution mixture of 3.0 mL of 1 M SbCl_3 in acetone, 25 mL of a 1 M $\text{Na}_2\text{S}_2\text{O}_3$ aqueous solution, and 72 mL of deionized water. The orange-colored amorphous Sb_2S_3 deposited on the TiO_2 NRs film was then heat-treated at 330 °C for 30 min in an N_2 atmosphere to convert into crystalline phase (stibnite). Upon completion of heat-treatment, we cooled it to room temperature in air.

Device Fabrication. The Sb_2S_3 -SPECs were assembled by sandwiching the $\text{Sb}_2\text{S}_3/\text{TiO}_2$ NRs/bl- TiO_2 /FTO substrate and Pt-coated counter electrode by a 60 μm thick thermal adhesive film spacer (Surllyn, DuPont). The Pt-coated counter electrodes were prepared by dropping a 5 mM solution of H_2PtCl_6 in isopropanol onto an FTO glass substrate and then heating them up to a temperature of 400 °C for 10 min. The cobalt electrolyte synthesized through the literature¹⁵ was injected by a vacuum backfilling process and sealed. The used cobalt electrolyte was 0.5 M $\text{Co(II)}(o\text{-phen})_3(\text{TFSI})_2$, 0.05 M $\text{Co(III)}(o\text{-phen})_3(\text{TFSI})_3$, and 0.2 M lithium perchlorate mixed in a 6:4 v/v ethylenecarbonate/acetonitrile solvent. Here *o*-phen and TFSI stand for 1,10-phenanthroline and bis(trifluoromethanesulfonyl) imide. Finally, we made lead contact pads on both sides of the electrode using an ultrasonic soldering iron (MBR electronics, USS-9200) to improve

electrical contacts. The active area of all devices was fixed to 0.196 cm^2 .

Blank Samples. For the comparison, the Sb_2S_3 -sensitized blank samples were also prepared by constructing two-device FTO/bl- TiO_2 / TiO_2 NRs/cobalt electrolyte and FTO/bl- TiO_2 / TiO_2 NRs/P3HT/cobalt electrolyte.

Characterization of Device Performance. The current density–voltage (J – V) characteristics of the Sb_2S_3 -SPECs were measured using a sourcemeter (Keithley 2420) and a calibrated Si-reference cell (certified by NREL) under 1 sun (100 mW/cm^2) AM 1.5G illumination by a solar simulator (Class A, 9119SA; Newport). The external quantum efficiency (EQE) was measured using a light source (300 W xenon lamp, 66902; Newport) aligned with a monochromator (Cornerstone 260; Newport) and a multimeter (Keithley 2002). All J – V curves were measured by masking them with 0.096 cm^2 metal mask.

3. RESULTS AND DISCUSSION

Figure 1a is a schematic device architecture composed of FTO/bl- TiO_2 / TiO_2 NRs/ Sb_2S_3 /P3HT/cobalt electrolyte. Upon illumination of external light, the electron–hole pairs are generated in Sb_2S_3 sensitizer with fast transfer of the generated

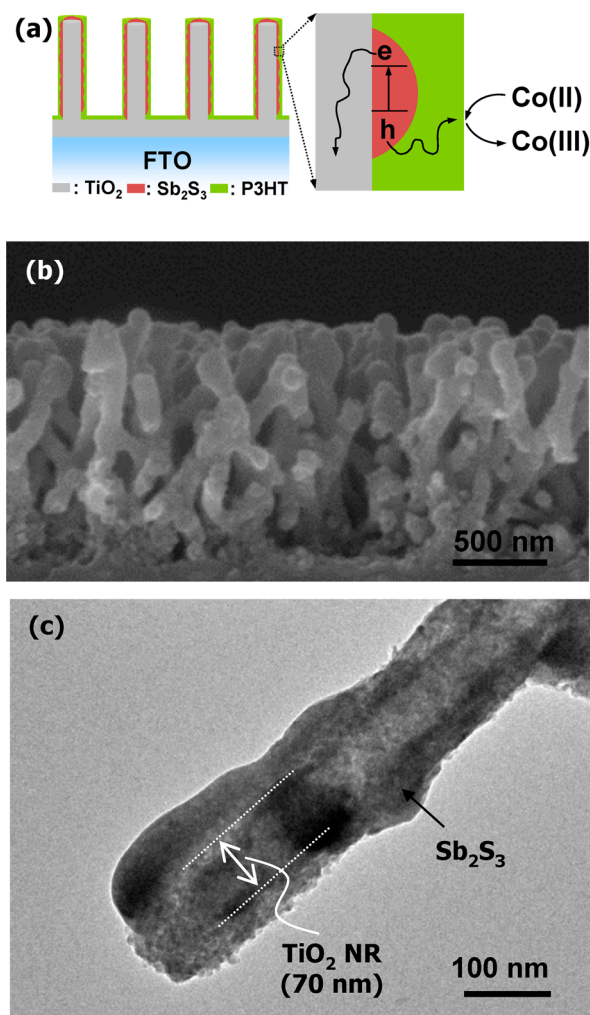


Figure 1. (a) Schematic illustration of device architecture, (b) SEM cross-sectional image of $\text{Sb}_2\text{S}_3/\text{TiO}_2$ NRs/bl- TiO_2 /FTO, and (c) TEM image of $\text{Sb}_2\text{S}_3/\text{TiO}_2$ NR.

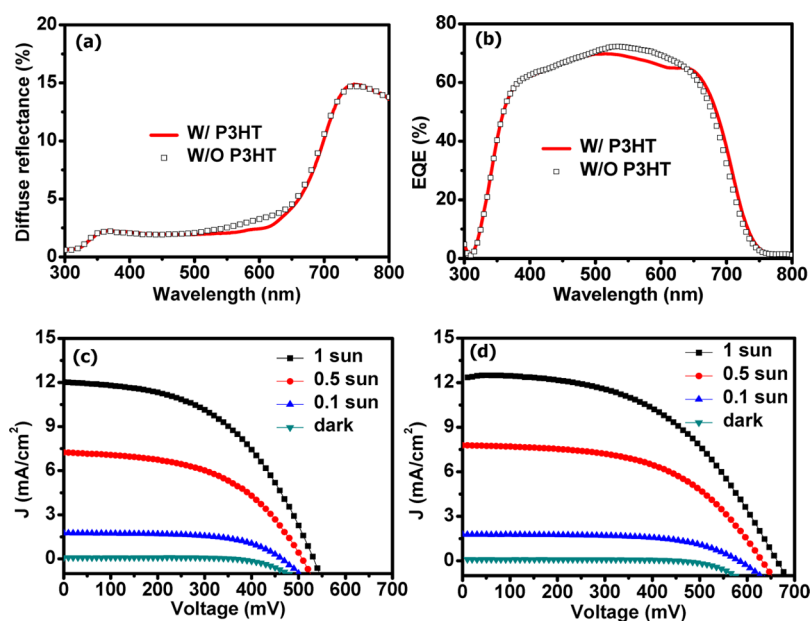


Figure 2. (a) Diffuse reflectance and (b) EQE spectra of Sb_2S_3 -SPEC with (W/P3HT) and without (W/O P3HT) P3HT hole buffer interlayer; photocurrent density–voltage (J – V) curves of W/O P3HT (c) and W/P3HT device (d) with illuminated sun intensity.

electrons to TiO_2 NRs electrode. At the same time, the generated holes are charge-transferred to P3HT hole conducting layer and then are regenerated by accepting electrons from Co(II) redox shuttles. The oxidized Co(II) to Co(III) redox shuttles are converted to Co(II) by accepting electrons of Pt counter electrode that come from the FTO electrode through external circuit. Figure 1b exhibits a cross-sectional SEM image of FTO/bl- TiO_2 / TiO_2 NRs/ Sb_2S_3 , clearly indicating that the sufficient pore space among TiO_2 NRs still remains even after Sb_2S_3 deposition. Apparently, the surface of 1 μm thick TiO_2 NRs seems to be coated by Sb_2S_3 , and macroporous morphology is well-developed. A TEM image in Figure 1c shows the morphology of Sb_2S_3 coated on TiO_2 NRs exhibiting that the surface of TiO_2 NRs (~ 70 nm in diameter) was fully covered by Sb_2S_3 .

Figure 2a shows diffuse reflectance of Sb_2S_3 -SPECs with (W/P3HT) and without P3HT interlayer (W/O P3HT). The spectra exhibit that both cells have same absorption up to 450 nm in a wavelength due to strong absorption of Sb_2S_3 , and the Sb_2S_3 -SPEC with P3HT interlayer has additional absorption in a wavelength range of 450–650 nm owing to the absorption of P3HT. The EQE is a product of light harvesting, charge separation, and charge collection efficiency. Therefore, the Sb_2S_3 -SPEC with P3HT is expected to hold better EQE value due to slightly stronger absorption than the Sb_2S_3 -SPEC without P3HT. Contradictively the Sb_2S_3 -SPEC without P3HT interlayer exhibited slightly better EQE values, especially at a wavelength range of 450–650 nm, as shown in Figure 2b. This phenomenon is caused by the fact that the generated charge carriers in the P3HT interlayer by light absorption cannot be effectively harvested to TiO_2 NRs through the Sb_2S_3 intermediate. In other words, the absorption by pure Sb_2S_3 in W/P3HT sample is lower than that in W/O P3HT sample because the incident light into the device is attenuated along the depth direction by the absorption to Sb_2S_3 and P3HT. In a previous report,²⁴ it was found that the generated charge carriers in P3HT can partially be transferred into TiO_2 , but they cannot be effectively collected to TiO_2 through Sb_2S_3

intermediate. This slight reduction of EQE spectrum in a wavelength range of 450–650 nm might be associated with the morphology of TiO_2 NRs/ Sb_2S_3 because the P3HT cannot be directly connected to the TiO_2 NRs owing to fully covering by Sb_2S_3 on the surface of TiO_2 NRs. The photocurrent density–voltage (J – V) characteristics of Sb_2S_3 -SPEC with and without P3HT with illuminated sun intensity are compared in Figure 2c,d, and their performances are summarized in Table 1. The

Table 1. Summary of Device Performance of Sb_2S_3 -SPEC with (W/P3HT) and without (W/O P3HT) P3HT Interlayer

	sun intensity (mW/cm^2)	J_{sc} (mA/cm^2)	V_{oc} (mV)	FF (%)	η (%)
W/O P3HT	100	12.0	530	49.5	3.2
	50	7.2	510	50.5	3.7
	10	1.8	460	61.0	4.9
W/P3HT	100	12.2	667	51.1	4.2
	50	7.8	627	53.8	5.2
	10	1.8	586	60.9	6.3

short circuit current density (J_{sc}) and fill factor (FF) of Sb_2S_3 -SPEC with (W/P3HT: $J_{\text{sc}} = 12.2$ mA/cm^2 , FF = 51.1%) and without P3HT interlayer (W/O P3HT: $J_{\text{sc}} = 12.0$ mA/cm^2 , FF = 49.5%) exhibit almost the same value, but the open circuit voltage (V_{oc}) of W/P3HT device (667 mV) shows a significantly higher value than W/O P3HT device (530 mV). Accordingly, the overall power conversion efficiency (η) is dominated by the different V_{oc} of the two devices, and the W/P3HT device (4.2%) has substantially better device performance than the W/O P3HT device (3.2%) at 1 sun illumination. In addition, it is also expected that the P3HT interlayer may reduce the mass transport problem of cobalt redox electrolyte in the macropore of TiO_2 NRs as described in previous report.²⁹ However, such effect does not seem to affect greatly the enhancement of device performance in TiO_2 NRs system because the J_{sc} still exhibits nonlinearity with illuminated sun intensity. This might be associated with the fact that the Sb_2S_3

is fully covered on the surface of TiO₂ NRs of which the effective surface area will not be further extended by the addition of P3HT interlayer, whereas it is expected that the P3HT interlayer will extend the effective surface area contacting cobalt electrolyte in dot-like Sb₂S₃ deposited on mesoscopic TiO₂ electrode. Hence, the enhanced device performance seems to be mainly attributed to the improved V_{oc} , which may associate with the backward recombination.

To elucidate why the W/P3HT device has higher open circuit voltage than the W/O P3HT device, we measured electrochemical impedance spectroscopy (EIS) with applied bias voltage under dark condition. Figure 3a shows

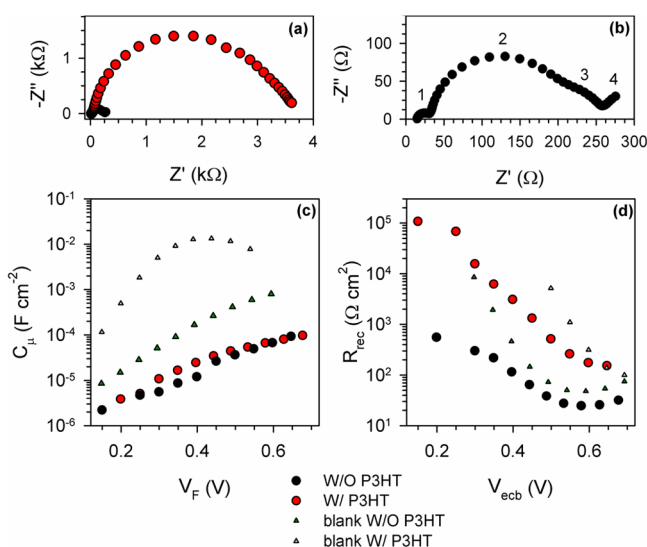


Figure 3. EIS analysis of W/P3HT and W/O P3HT device. (a) Representative Nyquist plots at 450 mV of applied bias voltage in dark state. (b) Zoom of panel a for W/O P3HT device. The four features detected in the spectra are labeled. (c) Chemical capacitance and (d) recombination resistance of devices.

representative complex plane impedance plots of W/P3HT and W/O P3HT device at 450 mV of applied bias voltage in dark state. Figure 3b presents a zoom of Figure 3a for W/O P3HT device. It is interesting to note that the impedance spectra present higher complexity than the current spectra reported for D-SPECs³² or QD SPECs.³³ The conventional pattern observed in sensitized solar cells presents as maximum three arcs: (i) at high frequencies an arc due to the charge transfer at the counter electrode, arc labeled 1 in Figure 3b; (ii) at intermediated frequencies an arc due to the recombination process at the TiO₂/absorber/electrolyte interface coupled to the chemical capacitance of TiO₂, arc labeled 2 in Figure 3b; and (iii) at lower frequencies an arc related with the diffusion process at the electrolyte, arc labeled 4 in Figure 3b. A wider frequency range is needed to observe clearly how this last arc closes to the real axis. The samples analyzed in this work present an additional feature: an arc labeled 3 in Figure 3b. This new feature can be attributed to Sb₂S₃ absorber because it is not observed in the blank samples without absorber. In this sense, a first hypothesis is that the origin of this feature is due to an alternative recombination pathway through surface states in Sb₂S₃. The analysis of this hypothesis is not straightforward because it introduces circuit elements that are not associated either in series or in parallel.³⁴ This complete study is under current research, and it is not within the scope of the present

paper. Here we aim to discern the origin of the higher V_{oc} observed for the W/P3HT cell in comparison with W/O P3HT sample; therefore, in a first approximation, we have fitted only the first part of the impedance spectra, arcs 1 and 2 in Figure 3b.^{32,33} This analysis has allowed us to obtain the chemical capacitance, C_{μ} and the recombination resistance, R_{rec} of the studied cells; see Figure 3c,d, respectively.

The fact that chemical capacitances overlap in Figure 3c indicates that both W/P3HT and W/O P3HT samples present the same position of TiO₂ conduction band (CB) position because no significant shift is observed between them. This shows that P3HT does not contribute an additional surface dipole so that the higher V_{oc} observed for W/P3HT cannot be attributed to an upward displacement of the TiO₂ CB. C_{μ} is plotted against the voltage drop in the sensitized electrode V_F , where the effect of the voltage drop in the series resistance is removed.³⁵ Conversely, note that the deposition of Sb₂S₃ sensitizer moves up the TiO₂ CB in comparison with the blank cells, as it can be appreciated by the shift in the capacitance. We think that the significant CB shift by the addition of Sb₂S₃ on TiO₂ NRs may be associated with the fact that the TiO₂ NRs are formed by ZnO NRs sacrificial template because it was reported that the CB of ZnO NRs in the CdSe/ZnO NRs device is greatly dependent on the CdSe deposited on ZnO NRs having different length,³⁵ whereas the CB was not significantly changed in Sb₂S₃ deposited on mesoscopic TiO₂ (pure TiO₂).^{25,36} On the other hand, an analysis of the recombination resistance (Figure 3d) gives two important conclusions: (i) the presence of Sb₂S₃ sensitizer enhances the recombination rate (decreases the recombination resistance) and (ii) W/P3HT presents lower recombination rate than W/O P3HT, indicating that the observed V_{oc} enhancement can be unambiguously attributed to a reduction in the backward recombination. Note that in Figure 3d the effect of the different TiO₂ CB position is removed, representing R_{rec} against the equivalent common CB, V_{ecb} (see the supporting Figure S1 for the calculation of V_{ecb}).³⁵

The increase in recombination rate with the presence of Sb₂S₃ sensitizer is in good agreement with previously reported results.^{25,36} This result indicates that Sb₂S₃ acts as a recombination center and further improvement of the solar cell efficiency could be expected if this recombination pathway is suppressed.

4. CONCLUSIONS

We could fabricate the efficient Sb₂S₃-SPEC with 4.2% of power conversion efficiency at 1 sun illumination, owing to the macroporous TiO₂ NRs structure and the P3HT interlayer. From the EIS analysis, we found that the P3HT interlayer enables the W/P3HT device to exhibit much larger R_{ct} than the W/O P3HT device and consequently reduces the recombination rate (with no effect in the TiO₂ CB position). Accordingly, the inserted P3HT interlayer greatly enhances the open circuit voltage of Sb₂S₃-SPECs owing to the reduced backward recombination and CB tuning of TiO₂. We believe that this new device architecture having P3HT interlayer will be extended to general inorganic semiconductor- or QD-SPECs and thus will be helpful to improve the device efficiency.

■ ASSOCIATED CONTENT

Supporting Information

C_{μ} - V_{ecb} graphs for the calculation of V_{ecb} . This material is available free of charge via the Internet at <http://pubs.acs.org>.

■ AUTHOR INFORMATION

Corresponding Author

*E-mail: seoksi@kriect.re.kr (S.I.S.), sero@fca.uji.es (I.M.-S.), and bisquert@fca.uji.es (J.B.).

Author Contributions

[§]These two authors have equally contributed to this study.

Notes

The authors declare no competing financial interest.

■ ACKNOWLEDGMENTS

This study was supported by the Global Research Laboratory (GRL) Program and the Global Frontier R&D Program on Center for Multiscale Energy System funded by the National Research Foundation under the Ministry of Education, Science and Technology of Korea and by a grant from the KRICT 2020 Program for Future Technology of the Korea Research Institute of Chemical Technology (KRICT), Republic of Korea. The work is also partially supported by the “Institute of Nanotechnologies for Clean Energies”, funded by the Generalitat Valenciana under project ISIC/2012/008. We acknowledge support by projects from Ministerio de Economía y Competitividad of Spain (Consolider HOPE CSD2007-00007, JES-NANOSOLAR PLE2009-0042) and Generalitat Valenciana (PROMETEO/2009/058).

■ REFERENCES

- (1) Grätzel, M.; O' Regan, B. *Nature* **1991**, *353*, 737–740.
- (2) Nazeeruddin, M. K.; Angelis, F. D.; Fantacci, S.; Selloni, A.; Viscardi, G.; Liska, P.; Ito, S.; Takeru, B.; Grätzel, M. *J. Am. Chem. Soc.* **2005**, *127*, 16835–16847.
- (3) Gao, F.; Wang, Y.; Zhang, J.; Shi, D.; Wang, M.; Humphry-Baker, R.; Wang, P.; Zakeeruddin, S. M.; Grätzel, M. *Chem. Commun.* **2008**, *23*, 2635–2637.
- (4) Bisquert, J. *ChemPhysChem* **2011**, *12*, 1633–1636.
- (5) Feldt, S. M.; Gibson, E. A.; Gabrielsson, E.; Sun, L.; Boschloo, G.; Hegfeldt, A. *J. Am. Chem. Soc.* **2010**, *132*, 16714–16724.
- (6) Yella, A.; Lee, H.-W.; Tsao, H. N.; Yi, C.; Chandiran, A. K.; Nazeeruddin, M. K.; Diao, E. W.-G.; Yeh, C.-Y.; Zakeeruddin, S. M.; Grätzel, M. *Science* **2011**, *334*, 629–634.
- (7) Yum, J.-H.; Baranoff, E.; Kessler, F.; Moehl, T.; Ahmad, S.; Bessho, T.; Marchioro, A.; Ghadiri, E.; Moser, J.-E.; Yi, C.; Nazeeruddin, M. K.; Grätzel, M. *Nat. Commun.* **2012**, *3*, 631:1–8.
- (8) Nozik, A. J. *Chem. Phys. Lett.* **2008**, *457*, 3–11.
- (9) Lee, Y.-L.; Lo, Y.-S. *Adv. Funct. Mater.* **2009**, *19*, 604–609.
- (10) Shalom, M.; Dor, S.; Rühle, S.; Grinis, L.; Zaban, A. *J. Phys. Chem. C* **2009**, *113*, 3895–3898.
- (11) Kamat, P. V. *J. Phys. Chem. C* **2008**, *112*, 18737–18753.
- (12) Sangtra, P. K.; Kamat, P. V. *J. Am. Chem. Soc.* **2012**, *134*, 2508–2511.
- (13) Lee, Y. H.; Im, S. H.; Rhee, J. H.; Lee, J.-H.; Seok, S. I. *ACS Appl. Mater. Interfaces* **2010**, *2*, 1648–1652.
- (14) Pan, Z.; Zhang, H.; Cheng, K.; Hou, Y.; Hua, J.; Zhong, X. *ACS Nano* **2012**, *6*, 3982–3991.
- (15) Lee, H. J.; Chen, P.; Moon, S.-J.; Sauvage, F.; Sivula, K.; Bessho, T.; Gamelin, D. R.; Comte, P.; Zakeeruddin, S. M.; Seok, S. I.; Grätzel, M.; Nazeeruddin, M. K. *Langmuir* **2009**, *25*, 7602–7608.
- (16) Im, S. H.; Kim, H.-j.; Kim, S. W.; Kim, S.-W.; Seok, S. I. *Energy Environ. Sci.* **2011**, *4*, 4181–4186.
- (17) Braga, A.; Giménez, S.; Concina, I.; Vomiero, A.; Mora-Seró, I. *J. Phys. Chem. Lett.* **2011**, *2*, 454–460.
- (18) Itzhak, Y.; Nitssoo, O.; Page, M.; Hodes, G. *J. Phys. Chem. C* **2009**, *113*, 4254–4256.
- (19) Moon, S.-J.; Itzhak, Y.; Yum, J.-H.; Zakeeruddin, S. M.; Hodes, G.; Grätzel, M. *J. Phys. Chem. Lett.* **2010**, *1*, 1524–1527.
- (20) Liu, C. P.; Wang, H. E.; Ng, T. W.; Chen, Z. H.; Zhang, W. F.; Yan, C.; Tang, Y. B.; Bello, I.; Martinu, L.; Zhang, W. J.; Jha, S. K. *Phys. Status Solidi B* **2012**, *249*, 627–633.
- (21) Gui, E. L.; Kang, A. M.; Pramana, S. S.; Yantara, N.; Mathews, N.; Mhaisalkar, S. *J. Electrochem. Soc.* **2012**, *159*, B247–B250.
- (22) Chang, J. A.; Rhee, J. H.; Im, S. H.; Lee, Y. H.; Kim, H.-J.; Seok, S. I.; Nazeeruddin, M. K.; Grätzel, M. *Nano Lett.* **2010**, *10*, 2609–2612.
- (23) Im, S. H.; Lim, C.-S.; Chang, J. A.; Lee, Y. H.; Maiti, N.; Kim, H.-j.; Nazeeruddin, M. K.; Grätzel, M.; Seok, S. I. *Nano Lett.* **2011**, *11*, 4789–4793.
- (24) Chang, J. A.; Im, S. H.; Lee, Y. H.; Kim, H.-j.; Lim, C.-S.; Heo, J. H.; Seok, S. I. *Nano Lett.* **2012**, *12*, 1863–1867.
- (25) Boix, P. P.; Larramona, G.; Jacob, A.; Delatouche, B.; Mora-Seró, I.; Bisquert, J. *J. Phys. Chem. C* **2012**, *116*, 1579–1587.
- (26) Nair, M. T. S.; Peña, Y.; Campos, J.; García, V. M.; Nair, P. K. *J. Electrochem. Soc.* **1998**, *145*, 2113–2120.
- (27) Messina, S.; Nairand, M. T. S.; Nair, P. K. *Thin Solid Films* **2007**, *515*, 5777–5782.
- (28) Messina, S.; Nair, M. T. S.; Nair, P. K. *Thin Solid Films* **2009**, *517*, 2503–2507.
- (29) Im, S. H.; Kim, H.-j.; Rhee, J. H.; Lim, C.-S.; Seok, S. I. *Energy Environ. Sci.* **2011**, *4*, 2799–2902.
- (30) Lim, C.-S.; Im, S. H.; Rhee, J. H.; Lee, Y. H.; Kim, H.-j.; Maiti, N.; Kang, Y.; Chang, J. A.; Nazeeruddin, M. K.; Grätzel, M.; Seok, S. I. *J. Mater. Chem.* **2012**, *22*, 1107–1111.
- (31) Yodyingyong, S.; Zhou, X.; Zhang, Q.; Triampo, D.; Xi, J.; Park, K.; Limketkai, B.; Cao, G. *J. Phys. Chem. C* **2010**, *114*, 21851–21855.
- (32) Fabregat-Santiago, F.; Garcia-Belmonte, G.; Mora-Seró, I.; Bisquert, J. *Phys. Chem. Chem. Phys.* **2011**, *13*, 9083–9118.
- (33) González-Pedro, V.; Xu, X.; Mora-Seró, I.; Bisquert, J. *ACS Nano* **2010**, *4*, 5783–5790.
- (34) Bisquert, J. *J. Electroanal. Chem.* **2010**, *646*, 43–51.
- (35) Fabregat-Santiago, F.; Garcia-Belmonte, G.; Mora-Seró, I.; Bisquert, J. *Phys. Chem. Chem. Phys.* **2011**, *13*, 9083–9118.
- (36) Boix, P. P.; Lee, Y. H.; Fabregat-Santiago, F.; Im, S. H.; Mora-Seró, I.; Bisquert, J.; Seok, S. I. *ACS Nano* **2012**, *6*, 873–880.